Journal of Luminescence 246 (2022) 118828

Contents lists available at ScienceDirect

Journal of Luminescence

journal homepage: www.elsevier.com/locate/jlumin

Tm,Ho:Ca(Gd,Lu)AlO_4 crystals: Crystal growth, structure refinement and Judd-Ofelt analysis

Zhongben Pan [a,b], Pavel Loiko [c], Sami Slimi [d], Hualei Yuan [e], Yicheng Wang [b], Yongguang Zhao [b,f], Patrice Camy [c], Elena Dunina [g], Alexey Kornienko [g], Liudmila Fomicheva [h], Li Wang [b], Weidong Chen [b,i], Uwe Griebner [b], Valentin Petrov [b], Rosa Maria Solé [d], Francesc Díaz [d], Magdalena Aguiló [d], Xavier Mateos [d,1,*]

[a] School of Information Science and Engineering, Shandong University, Qingdao 266237, China
[b] Max Born Institute for Nonlinear Optics and Short Pulse Spectroscopy, Max-Born-Str. 2a, 12489, Berlin, Germany
[c] Centre de Recherche sur les Ions, les Matériaux et la Photonique (CIMAP), UMR 6252 CEA-CNRS-ENSICAEN, Université de Caen Normandie, 6 Boulevard du Maréchal Juin, 14050, Caen Cedex 4, France
[d] Universitat Rovira i Virgili, Dept. Química Física i Inorgànica, FiCMA-FiCNA, Marcel·li Domingo, 1, 43007, Tarragona, Spain
[e] Institute of Chemical Materials, China Academy of Engineering Physics, Mianyang, 621900, China
[f] Jiangsu Key Laboratory of Advanced Laser Materials and Devices, Jiangsu Normal University, 221116, Xuzhou, China
[g] Vitebsk State Technological University, 72 Moskovskaya Ave., 210035, Vitebsk, Belarus
[h] Belarusian State University of Informatics and Radioelectronics, 6 Brovka St., 220027, Minsk, Belarus
[i] Fujian Institute of Research on the Structure of Matter, Chinese Academy of Sciences, 350002 Fuzhou, China

ARTICLE INFO

Keywords:
Aluminate crystals
Czochralski growth
Structure refinement
Raman spectra
Optical absorption
Judd-Ofelt theory

ABSTRACT

"Mixed" calcium rare-earth aluminate laser host crystals Ca(Gd,Lu)AlO_4 (CALGLO) with up to 10.8 at.% Lu codoped with Tm^{3+} and Ho^{3+} ions are grown by the Czochralski method along the [001] direction. The segregation of rare-earth ions is studied. The crystal structure is refined by the Rietveld method. Tm,Ho:Ca(Gd,Lu)AlO_4 crystallizes in the tetragonal system (sp. gr. *I4/mmm*) exhibiting a K_2NiF_4 type structure. The lattice constants are a = 3.6585(6) Å and c = 11.9660(9) Å for a crystal with a composition of $Ca(Gd_{0.8947}Lu_{0.0551}Tm_{0.0448}Ho_{0.0054})AlO_4$. The stability of Ca(Gd,Lu)AlO_4 solid-solutions is discussed. The polarized Raman spectra are measured, revealing a most intense mode at 311 cm^{-1} and a maximum phonon frequency of ~650 cm^{-1}. The polarized absorption spectra are measured. The transition intensities for the Ho^{3+} ion are analyzed using the modified Judd-Ofelt theory accounting for configuration interaction.

1. Introduction

Calcium rare-earth aluminates $CaLnAlO_4$ where Ln stands for Gd or Y (denoted as CALGO/CGA and CALYO/CYA, respectively) are attractive laser host crystals [1–3]. They crystallize in a tetragonal class having a K_2NiF_4-type structure and exhibit structural disorder: the Ca^{2+} and $Gd^{3+}|Y^{3+}$ cations are statistically distributed over the same Wyckoff site (4*e*, C_{4v}-symmetry) [4,5]. As a result, $CaLnAlO_4$ doped with laser-active trivalent rare-earth ions (RE^{3+}) such as Yb^{3+}, Tm^{3+}, Ho^{3+}, *etc.*, exhibit significant inhomogeneous broadening of spectral bands [6]. Despite their disordered nature, the $CaLnAlO_4$ crystals provide good thermal properties, such as high thermal conductivity (~6.7 $Wm^{-1}K^{-1}$ for $CaGdAlO_4$) with moderate dependence on the RE^{3+} doping concentration, weak anisotropy of thermal expansion and negative thermo-optic coefficients leading to almost "athermal" behavior [7]. Tetragonal $CaLnAlO_4$ crystals exhibit natural birefringence [8] and enable polarized laser emission [9]. Due to the presence of the substitutional rare-earth site, the doping of $CaLnAlO_4$ crystals is relatively easy. Finally, particularly for Ln = Gd and Y, the $CaLnAlO_4$ compounds melt congruently (at ~1750 °C in the former case), so that large crystals can be grown relatively easy by the conventional Czochralski (Cz) method [10].

The reported thermal and spectroscopic properties of RE^{3+}-doped $CaLnAlO_4$ rendered these crystals excellent candidates for generation and amplification of ultrashort laser pulses [11,12], including the

* Corresponding author. Universitat Rovira i Virgili, Dept. Química Física i Inorgànica, FiCMA-FiCNA-EMaS, Marcel·li Domingo, 1, 43007, Tarragona, Spain.
E-mail address: xavier.mateos@urv.cat (X. Mateos).
[1] Serra Húnter Fellow.

https://doi.org/10.1016/j.jlumin.2022.118828
Received 7 June 2021; Received in revised form 22 February 2022; Accepted 6 March 2022
Available online 7 March 2022

high-power regime [13] (e.g., thin-disk lasers [14,15]). In the past decades, the research activity mainly focused on Yb^{3+}-doped crystals corresponding to the spectral range of ~1 μm [11–15]. More recently, the interest shifted towards the eye-safe spectral range of ~2 μm [16,17]. The laser emission at ~2 μm is typically achieved using thulium (Tm^{3+}) and/or holmium (Ho^{3+}) dopant ions. The growth and spectroscopic characterization of singly doped and Tm^{3+},Ho^{3+}-codoped $CaGdAlO_4$ and $CaYAlO_4$ crystals were reported in Refs. [3,18]. Furthermore, such materials were proven to be capable of generating femtosecond pulses at ~2 μm [16,17].

The $CaLnAlO_4$ crystals belong to a big class of oxides with a general chemical formula of $ABCO_4$, where $A^{2+} = Ca^{2+}$ or Sr^{2+}, B^{3+} is a rare-earth cation, and $C^{3+} = Al^{3+}$ or Ga^{3+} [19]. Not all the possible $ABCO_4$ compositions are stable, exhibit the desired K_2NiF_4-type tetragonal structure and melt congruently. Other known compositions satisfying these conditions are $SrLaAlO_4$ and $SrLaGaO_4$ [20,21]. The search for other compositions of $ABCO_4$ crystals (and, in particular, $CaLnAlO_4$ ones) will help to improve the thermal and spectroscopic properties. Another option is the growth of "mixed" crystals (solid solutions) leading to compositional disorder and hence to additional broadening of the spectral bands of laser-active RE^{3+} dopant ions. As for the $CaLnAlO_4$ crystals, the Cz growth of stoichiometric compounds with other host-forming cations was reported only for Ln = Nd [4,22], Dy [23] and Tb [24]. However, all these ions are optically active and do not appear attractive for "mixed" crystals.

The lutetium ion (Lu^{3+}) is known as a passive host-forming cation for many oxide materials such as garnets ($Lu_3Al_5O_{12}$), sesquioxides (Lu_2O_3), tungstates ($KLu(WO_4)_2$) or perovskites ($LuAlO_3$). Due to the closeness of ionic radii of Lu^{3+} and Yb^{3+} or Tm^{3+} ions, Lu-based oxides (as compared to their Gd-based counterparts) provide easier doping and weaker dependence of thermal properties on the doping level [25]. Unfortunately, so far, the $CaLuAlO_4$ compound has never been synthesized as a single crystal [26]. An alternative route can be the fabrication of a "mixed" material, e.g., $Ca(Gd,Lu)AlO_4$ with a partial substitution of Gd^{3+} by Lu^{3+}. First, this idea was exploited in Ref. [27] to produce Yb^{3+}-doped $Ca(Gd,Lu)AlO_4$ crystals (denoted as CLGA) with a maximum Lu^{3+} content of 5.5 at.%. Later, Tm^{3+}-doped crystals with a similar Lu^{3+} content were grown and their spectroscopic and laser properties were studied [28].

In the present work, we report on the first Cz growth of Tm^{3+},Ho^{3+}-codoped "mixed" $Ca(Gd,Lu)AlO_4$ (abbreviated: CALGLO) crystals preserving the tetragonal K_2NiF_4-type structure. These crystals feature increased Lu^{3+} content up to 10.8 at.% extending the understanding of solid-solution formation in the system $Ca(Gd_{1-x}Lu_x)AlO_4$.

2. Crystal growth

5 at.% Tm^{3+}, 0.5 at.% Ho^{3+} (in the melt) codoped $Ca(Gd_{1-x}Lu_x)AlO_4$ (where $x = 0.1$ or 0.2 corresponds to batches #1 and #2, respectively) single crystals were grown by the Cz method using an argon atmosphere in an iridium crucible. An automatic system was employed to control the boule diameter. The polycrystalline materials were obtained by solid-state reaction from a mixture of the starting materials, Al_2O_3, RE_2O_3 (where RE = Gd, Lu, Tm and Ho) (purity: 5 N) and $CaCO_3$ (purity: 4 N). For that, the raw materials taken in stoichiometric composition according to the following formula were well mixed, ground and firstly heated to 1173 K for 12 h (h) to decompose $CaCO_3$ using a platinum crucible. Once the crucible was cooled down to room temperature, the obtained mixture was pressed into pellets and again reheated to 1673 K for 30 h to synthesize polycrystalline materials.

$$2CaCO_3 + 0.05Tm_2O_3 + 0.005Ho_2O_3 + Al_2O_3 + xLu_2O_3 + (0.945 - x)Gd_2O_3 \rightarrow 2Ca(Gd_{0.945-x}Lu_x)Tm_{0.05}Ho_{0.005}AlO_4 + 2CO_2\uparrow$$

The synthesized polycrystalline material was placed in an iridium crucible and melted by an intermediate-frequency heater. A [001]-oriented undoped $CaGdAlO_4$ seed was used, the pulling rate varied from 0.5 to 2 mm/h and the crystal rotation speed was kept at 8–15 revolutions per minute (rpm). Once the growth was completed, the crystals were removed from the melt and slowly cooled down to room temperature (RT, 293 K) at a stepped rate of 15–25 K/h. The photographs of the as-grown crystal boules of Tm,Ho:CALGLO are shown in Fig. 1(a,c). They have a cylindrical shape with slightly varying cross-section along the length of the boule (about 3.0 cm). The cross-section of all the grown boules is rounded, no natural crystal planes are observed. The as-grown crystals exhibit brown-yellow coloration which is typical for aluminate crystals [29–31] and is assigned to interstitial oxygen ions. The crystal boules with high Lu^{3+} content show some small cracks at their shoulders. We attribute this to the flat shape of the shoulders, which causes much larger radiant area during the crystal growth and cooling process. Though small cracks exist in the crystal, the samples cut from the crystal are still of high optical quality. The coloration is greatly removed by annealing at 950 °C for 24 h under N_2 atmosphere with 5% H_2 (in oxygen-deficient conditions).

3. Experimental

The concentration of doping ions (Tm^{3+}, Ho^{3+} and Lu^{3+}) was measured by Inductively Coupled Plasma Mass Spectrometry (ICP-MS) using an Agilent® 8800 triple quadrupole ICP-MS analyzer.

The X-ray powder diffraction (XRD) patterns were measured at RT using a Bruker D2 Phaser diffractometer for diffraction angles 2θ in the range of 10–90° with Cu Kα1 radiation (1.54056 Å).

The crystal density was measured by the buoyancy method at 294 K, $\rho_{meas} = (m\rho_{water})/(m - m')$, where m and m' is the sample mass in air and in water, respectively, $\rho_{water} = 0.998$ g/cm^3 is the density of water. Each ρ_{meas} value was averaged for 3 different samples from the same batch.

For polarized Raman and absorption measurements, rectangular samples oriented along the crystallographic axes (***a***, ***c***) were prepared and polished (all lateral sides), as shown in Fig. 1(b,d). The polarized Raman spectra were measured using a confocal Raman microscope (Renishaw inVia) equipped with a × 50 objective, a set of a polarizer, an analyzer and a λ/2 plate, and a cut-on filter. The excitation wavelength was 514 nm (Ar^+ ion laser line).

The RT polarized absorption spectra in the range of 300–2200 nm were measured using a CARY 5000 (Varian) spectrophotometer equipped with a Glan-Taylor polarizer; the resolution (spectral bandwidth, SBW) was 0.2 nm. The IR transmission spectrum was measured using a Fourier transform infrared spectrometer (FTIR, model FI/IR 6700, Jasco).

4. Structural study

4.1. Crystal composition

The results on the concentration of doping ions (Tm^{3+}, Ho^{3+} and Lu^{3+}) are shown in Table 1. In particular, for batch #1, the actual doping levels were determined to be 4.48 at.% Tm, 0.54 at.% Ho and 5.51 at.% Lu corresponding to the stoichiometric chemical formula of $CaGd_{0.8947}Lu_{0.0551}Tm_{0.0448}Ho_{0.0054}AlO_4$. The ion densities amounted to $N_{Tm} = 5.54 \times 10^{20}$ cm^{-3} and $N_{Ho} = 0.66 \times 10^{20}$ cm^{-3}.

Let us analyze the segregation coefficients for three rare-earth ions, $K_{RE} = C_{crystal}/C_{melt}$, where $C_{crystal}$ and C_{melt} are the doping levels in the crystal and in the raw materials (in the melt), respectively. For Tm^{3+} and Ho^{3+} ions, they are close to unity, $K_{Tm} = 0.90$ and $K_{Ho} = 0.76$–1.07 and for Lu^{3+} ones, $K_{Lu} = 0.54$–0.55 is much smaller. In the parent compound, $CaGdAlO_4$, the host-forming Ca^{2+} and Gd^{3+} cations statistically occupy the same type of site (Wyckoff symbol: 4*e*, site symmetry: C_{4v}, coordination number (C.N.) by oxygen: IX). It is expected that all the dopant cations replace for the Gd^{3+} ones. The observed difference in the segregation coefficients can be understood from the point of view of mismatch of ionic radii, namely $R_{Tm} = 1.052$ Å, $R_{Ho} = 1.072$ Å and R_{Lu}

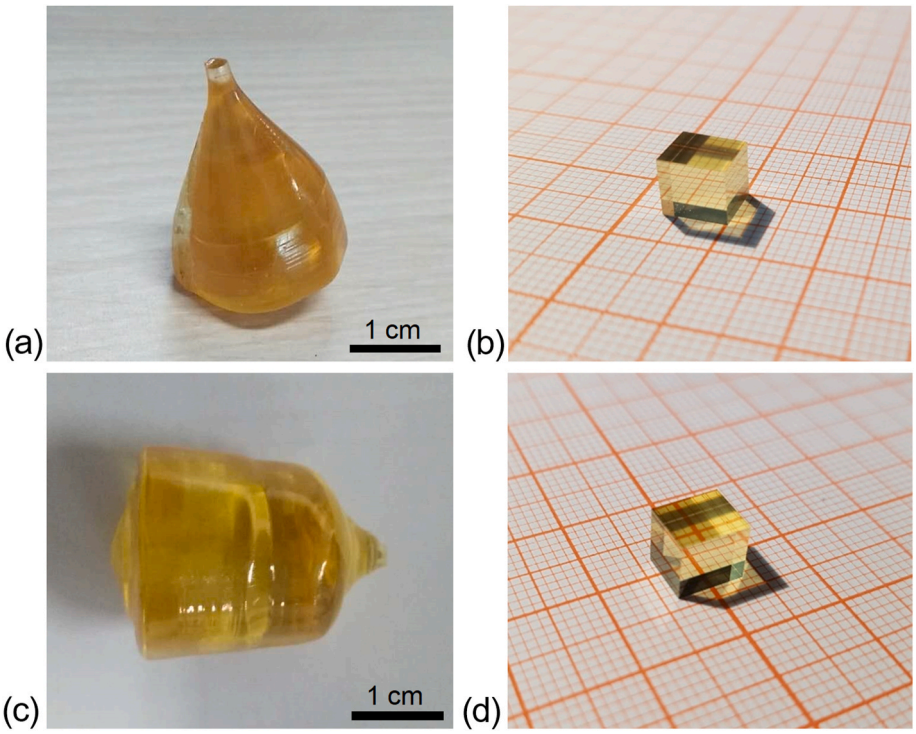

Fig. 1. (a–d) Photographs of the Tm,Ho:CALGLO single crystals grown by the Czochralski method: (a,c) as-grown crystal boules, (b,d) polished cubic samples oriented along crystallographic axes; (a,b) 5.5 at.% Lu^{3+}, (c,d) 10.8 at.% Lu^{3+} (in the crystal). The full chemical formulas are given in Table 1. The growth direction is along the [001] axis.

Table 1
Raw and actual compositions of the Tm,Ho:CALGLO crystals grown by the Czochralski method, K_{RE} – segregation coefficient.

Crystal	Batch #1	Batch #2
Raw composition		
Tm, at.%	5.0	5.0
Ho, at.%	0.5	0.5
Lu, at.%	10.0	20.0
Actual composition		
Tm, at.% [cm^{-3}]	4.48 [5.54×10^{20}]	4.50 [5.55×10^{20}]
Ho, at.% [cm^{-3}]	0.54 [0.66×10^{20}]	0.38 [0.47×10^{20}]
Lu, at.% [cm^{-3}]	5.51 [6.78×10^{20}]	10.80 [13.3×10^{20}]
Chemical formula	$CaGd_{0.8947}Lu_{0.0551}Tm_{0.0448}Ho_{0.0054}AlO_4$	$CaGd_{0.8432}Lu_{0.1080}Tm_{0.0450}Ho_{0.0038}AlO_4$
K_{Tm}	0.90	0.90
K_{Ho}	1.07	0.76
K_{Lu}	0.55	0.54

= 1.032 Å, compared with the larger R_{Gd} = 1.107 Å and especially R_{Ca} = 1.180 Å [32]. The results are compiled also in Fig. 2 where data on K_{RE} for other rare-earth ions in $CaGdAlO_4$ crystals from the literature [33–38] are added. The data were fitted using the following formula based on Onuma's principle [39]: $K_{RE} = K_0 - C(R_{RE} - R_{Gd})^2$ with the best-fit parameters $K_0 = 1.1 \pm 0.1$ and $C = 95 \pm 5$ $Å^{-2}$.

In the previous work on the parent $CaGdAlO_4$ crystals singly doped by Tm^{3+} and Ho^{3+} ions [18], lower segregation coefficients were reported, namely $K_{Tm} = 0.61$ and $K_{Ho} = 0.66$ (the crystal composition was analyzed by ICP atomic emission spectrometry). It seems that the addition of Lu^{3+} improves the segregation of Tm^{3+} and Ho^{3+} ions in $CaGdAlO_4$. We attribute this to much closer ionic radii of Lu^{3+} and the two above-mentioned dopant cations (as compared to Gd^{3+}). The slight variation of K_{Tm} and K_{Ho} values determined by analyzing crystals grown from batches #1 and #2 (which is more evident for Ho^{3+} because of the low doping level) is mainly due to the error of the IPC-MS method and to a less extent – to a certain distribution of dopants in the single crystals.

It is known that a solid-solution of isostructural compounds can be formed if the relative difference between the ionic radii of the host-forming cation H (Gd^{3+}, in our case) and the dopants D (Lu^{3+}, Tm^{3+}, Ho^{3+}, ion our case), expressed by the formula $\Delta_R = |(R_D - R_H)/R_H) \times 100\%$, does not exceed 15%. In our case, this parameter is maximum for Lu^{3+}, $\Delta_R = 6.8\%$, but the above-mentioned condition is still satisfied.

4.2. X-ray diffraction

The measured X-ray powder diffraction (XRD) patterns of the Tm,Ho:CALGLO crystals are shown in Fig. 3. In the same figure, we show the theoretical reflections from the Crystallography Open Database (COD) card #96-722-7258 for undoped $CaGdAlO_4$. The experimental XRD patterns match well the theoretical ones, indicating a single-phase nature of the material. The crystal structure was refined using the Rietveld method with the aim of the *match!* software, as shown in Fig. 4. The atomic coordinates from Ref. [30] were taken as a starting model for the Rietveld refinement. The obtained main crystallographic data and the refinement parameters are listed in Table 2. Tm,Ho:CALGLO crystallizes in the tetragonal system (sp. gr. D^{17}_{4h} - *I4/mmm*, No. 139) exhibiting a K_2NiF_4 type structure. For the crystal growth from the batch #1, the

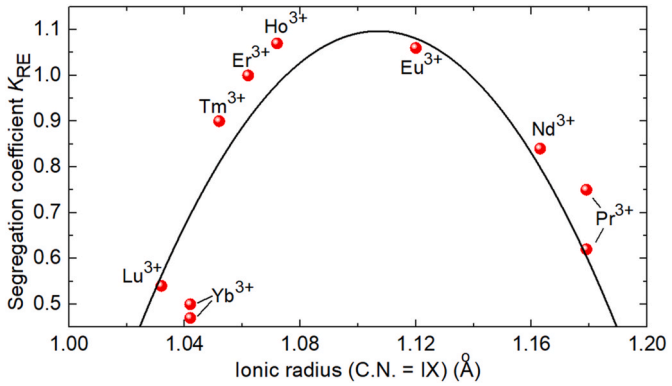

Fig. 2. Segregation coefficients of rare-earth ions (RE^{3+}) K_{RE} in $CaGdAlO_4$ crystals vs. their ionic radii for VIX-fold oxygen coordination (C.N. – coordination number), *circles* - experimental data (this work and Refs. [33–38]), *curve* – their fit according to the Onuma's principle [39], $K_{RE} = K_0 - C(R_{RE} - R_{Gd})^2$ where $K_0 = 1.1 \pm 0.1$ and $C = 95 \pm 5$ Å^{-2} (this work).

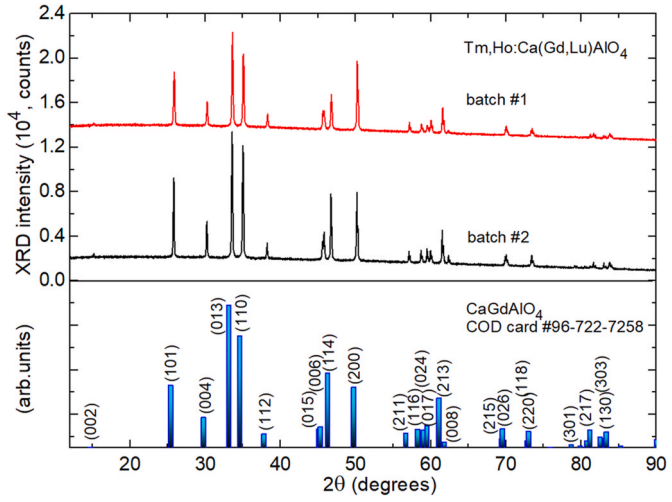

Fig. 3. X-ray powder diffraction (XRD) patterns of Tm,Ho:CALGLO crystals, *vertical bars* mark theoretical reflections for undoped $CaGdAlO_4$ (COD card #96-722-7258), *numbers* indicate the Miller's indices (*hkl*).

lattice constants $a = b = 3.6585$ (6) Å, $c = 11.9660(9)$ Å, the volume of the unit-cell $V = 160.167$ Å^3 (number of the formula units per unit-cell Z = 2). The calculated crystal density is then $\rho_{calc} = 6.010$ g/cm^3. The measured density ρ_{meas} amounted to 6.02 g/cm^3 (batch #1) and 6.08 g/cm^3 (batch #2), respectively, in agreement with the values calculated from the XRD data. The obtained lattice constants are slightly smaller than those for undoped $CaGdAlO_4$, $a = 3.6632(3)$ Å and $c = 11.998(2)$ Å [30], because of the smaller ionic radii of the dopant cations as compared to the host-forming ones.

The reliability factors obtained are listed in Table 2. For the crystal grown from batch #1, the weighted profile *R*-factor $R_{wp} = 2.82$, the expected *R*-factor $R_{exp} = 2.31$ and the Chi-squared $\chi^2 = (R_{wp}/R_{exp})^2 = 3.33$.

During the structure refinement, the fractional atomic coordinates in specific positions (*z* coordinates for the Wyckoff positions 4*e* in the considered structure) and the isotropic displacement parameters (B_{iso}) were optimized, Table 3. The site occupancy for the Wyckoff position 4*e* was taken assuming a random distribution of Ca^{2+} and RE^{3+} cations following the ratio of 1:1. Then, by considering the substitution of Gd^{3+} by RE^{3+} cations (Lu^{3+}, Tm^{3+}, Ho^{3+}) according to their actual doping levels described above, the site occupancy factors (O.F.) were calculated, Table 3. We have also tried to refine the occupancy factors of the

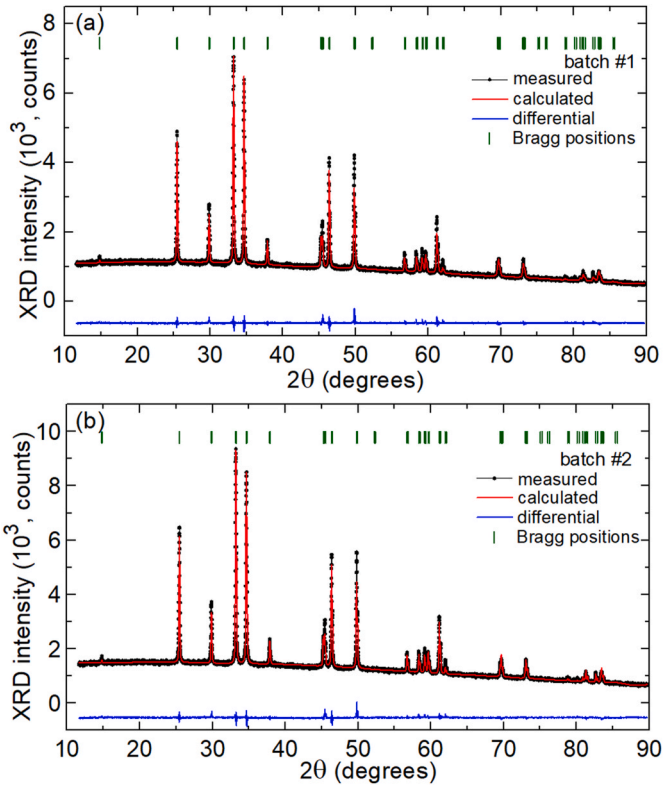

Fig. 4. (a,b) Rietveld refinement of the XRD patterns of Tm,Ho:CALGLO crystals: observed (*black*), calculated (red*)* and differential (*blue*) patterns, *vertical dashes* – Bragg reflections (*green*), growth batch: (a) #1 and (b) #2, cf. Table 1.

Table 2
Crystallographic data and Rietveld refinement parameters for Tm,Ho:CALGLO crystals.

Parameter	Value
System	Tetragonal
Space group (IT number)	D^{17}_{4h} - *I4/mmm* (No. 139)
Number of formula units	$Z = 2$
Point Group	4/mmm
Reduced Number of S.O.	8
General multiplicity	32
Centrosymmetry	Centric (−1 at origin)
Calculated density (g/cm^3)	6.010 (#1) 6.028 (#2)
Lattice constants *a*, *c* (Å)	3.6585 (6), 11.9660 (9) (#1) 3.6592 (4), 11.9689 (1) (#2)
$\alpha = \beta = \gamma$ (deg.)	90
Volume (Å^3)	160.167 (#1) 160.264 (#2)
2θ range (deg)	12–90
2θ step	0.02
Radiation	Cu-Kα1 ($\lambda = 1.5418$ Å)
No. of reflections	72
Refinement software	*match!* software
Reliability factors	$R_p = 2.82$, $R_{wp} = 4.22$, $R_{exp} = 2.31$ and $\chi^2 = 3.33$ (#1) $R_p = 2.57$, $R_{wp} = 3.87$, $R_{exp} = 2.31$ and $\chi^2 = 2.80$ (#2)

Wyckoff positions 4*e* (4*c*) and 2*a* occupied by O1 (O2) and Al atoms, respectively. This led to the O.F. values very close to unity.

A fragment of the crystal structure drawn using the VESTA software according to the determined set of atomic coordinates is shown in Fig. 5. The corresponding interatomic distances (Al – O, Ca|RE – O and Ca|RE – Ca|RE) are summarized in Table 4. Al^{3+} cations are located in 2*a* sites (symmetry: C_{4v}) and they are VI-fold oxygen coordinated forming

Table 3
Refined atomic coordinates (x, y, z) and isotropic displacement parameters B_{iso} determined via Rietveld refinement for Tm,Ho:CALGLO crystals and their estimated standard deviations.

Atoms	Site	x	y	z	O.F.	B_{iso}, Å^2
Batch #1						
Ca	4*e*	1/2	1/2	0.1402(0)	0.500	2.089(2)
Gd | Lu	4*e*	1/2	1/2	0.1402(0)	0.447 | 0.027	2.089(2)
Tm | Ho	4*e*	1/2	1/2	0.1402(0)	0.022 | 0.002	2.089(2)
Al	2*a*	0	0	0	1	0.467(8)
O1	4*e*	1/2	1/2	0.3304(0)	1	1.842(5)
O2	4*c*	0	1/2	0	1	1.863(3)
Batch #2						
Ca	4*e*	1/2	1/2	0.1404(0)	0.500	2.362(6)
Gd | Lu	4*e*	1/2	1/2	0.1404(0)	0.416 | 0.054	2.362(6)
Tm | Ho	4*e*	1/2	1/2	0.1404(0)	0.027 | 0.001	2.362(6)
Al	2*a*	0	0	0	1	0.763(9)
O1	4*e*	1/2	1/2	0.3317(0)	1	2.730(3)
O2	4*c*	0	1/2	0	1	1.980(5)

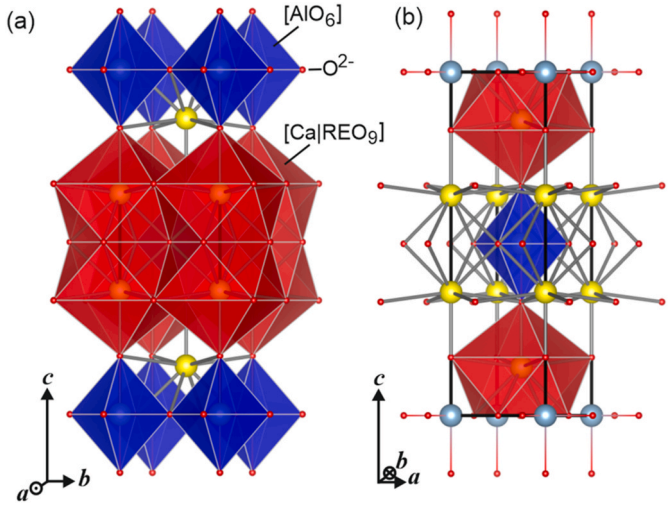

Fig. 5. Fragment of the structure of a Tm,Ho:CALGLO crystal, *black lines* mark the unit-cell, blue polyhedra – [AlO_6] and red polyhedra – [Ca|REO_9], where RE = Gd, Lu, Tm or Ho.

Table 4
Selected interatomic distances for Tm,Ho:CALGLO crystals.

Distances	Value (Å)	
	Batch #1	Batch #2
Al – O	O2 1.829(2) × 4	O2 1.829(6) × 4
	O1 2.028(4) × 2	O1 2.013(6) × 2
Ca|RE – O	O1 2.276(9) × 1	O1 2.289(8) × 1
	O2 2.482(0) × 4	O2 2.484(5) × 4
	O1′ 2.610(6) × 4	O1′ 2.608(7) × 4
Ca|RE – Ca|RE	3.355(2) × 1	3.361(8) × 1
	3.658(5) × 4	3.659(2) × 4
	3.687(5) × 4	3.684(1) × 4

distorted [AlO_6] octahedra elongated along the [001] direction. The distances from Al to two axial O1 atoms are 2.028(4) Å and thus longer than the "ideal" Al–O bond length (1.935 Å), whereas the distances to the four basal O2 atoms are 1.829(2) Å and thus shorter than the "ideal" bond length (here and below, the distances are specified for batch #1), Fig. 6. The Ca^{2+} | RE^{3+} cations statistically occupy the 4*e* sites (symmetry: C_{4v}) and they are IX-fold oxygen coordinated. There is one shorter (O1, 2.276(9) Å), four intermediate (O2, 2.482(0) Å) and four longer (O1′ 3.687(5) Å) distances in the [Ca|REO_9] polyhedra, Fig. 6, leading to a mono-capped tetragonal anti-prismatic geometry. The oxygen atoms are distributed over the 4*e* (O1) and 4*c* (O2) sites.

The structure of Tm,Ho:CALGLO is determined by a condensed framework of corner-sharing [AlO_6] and [Ca|REO_9] polyhedra. They form infinite layers parallel to the ***a*–*b*** plane. More generally, the structure of tetragonal (K_2NiF_4-type) $ABCO_4$ crystals can be divided into a sequence of layers running along the [001] direction with rock salt (S) and perovskite (P) structure [40]. In the case of Tm,Ho:CALGLO, the P and S "phases" comprise $REAlO_3$ and CaO, respectively.

In Fig. 7, we analyze the Al – O interatomic distances in [AlO_6] octahedra for various MM'AlO_4 crystals possessing the tetragonal K_2NiF_4-type structure [4]. The distances to axial and basal O atoms, as well as their average values increase with the mean ionic radius of the M^{2+} and M'^{3+} cations, so that the average distance approaches the "ideal" value of 1.935 Å, calculated from the ionic radii of VI-fold coordinated Al^{3+} (0.535 Å) and O^{2-} (1.40 Å) [32] (typically, the Al – O distances are invariant [4]). This distortion of the [AlO_6] octahedra occurs as the Al – O2 bond distance is constrained by the unit-cell dimensions (both Al and O2 are located in special positions, Table 3), while the Al – O1 distances are constrained by the lattice constant c and the variable z atomic coordinate.

The second coordination sphere of Ca^{2+} | RE^{3+} cations is composed of 9 nearest neighbor 4*e* sites, Fig. 8. The shortest metal-to-metal Ca|RE – Ca|RE distance is 3.355(2) Å (× 1), observed along the [u v w] = [001] direction. Other interactions correspond to intermediate distances of 3.658(5) Å (× 4) and longest distances of 3.687(5) Å × 4. The origin of the disorder is the second coordination sphere of RE^{3+} ions, namely the charge difference between the Ca^{2+} and RE^{3+} cations and the large difference in the metal-to-metal distances [6]. As only one apical site corresponds to the shortest Ca|RE – Ca|RE distance, it induces two families of local environment if it is occupied by Ca^{2+} or RE^{3+} cations. Each family contains surroundings with different distributions of Ca^{2+} and RE^{3+} cations over eight remaining 4*e* sites. This leads to significant inhomogeneous broadening of the spectral bands of optically active RE^{3+} cations. The introduction of Lu^{3+} further enhances the disorder, considering the difference in the ionic radii of Lu^{3+} and Gd^{3+}, which is expected to cause additional spectral broadening.

It is worth discussing the expected effect of RE^{3+} ions on the spectral line broadening. One may argue that the addition of optically active dopants (Tm^{3+} or Ho^{3+}) in high concentrations by itself can induce an additional "compositional" disorder. However, the doping level for both ions is limited by the detrimental energy-transfer upconversion capable of preventing the desired laser operation. In the (Tm^{3+}, Ho^{3+}) system, an optimum codoping ratio Ho/Tm between 1:10 and 1:5 is required to ensure a unidirectional $Tm^{3+} \rightarrow Ho^{3+}$ energy-transfer. These spectroscopic considerations limit in practice the actual doping levels for both ions. The Lu^{3+} cations are optically passive and thus do not induce unwanted spectroscopic processes. Moreover, the difference in the ionic radii in the pair Gd^{3+} | Lu^{3+} is larger than in the pairs Gd^{3+} | Tm^{3+}, Ho^{3+} which enhances the additional spectral broadening. The drawback is the lower segregation coefficient for Lu^{3+}.

Let us also discuss the terminological aspect of calling the grown crystals "mixed". Strictly speaking, they should be called a substitutional single-phase solid solution. The term "mixed" crystal exists as a synonym to solid solution materials, e.g., $A_{1-x}B_x$ if there are only two parent compounds. As explained above, we assume that Tm^{3+} and Ho^{3+} as dopants hardly affect the spectral broadening, while Lu^{3+} is the cation aimed to fulfil this task. There is no universal definition for the x parameter in $A_{1-x}B_x$ to distinguish the term "doping" from the "mixed" crystal or solid-solution. From the point of view of optics, the borderline can be defined as the minimum value inducing a noticeable change on the spectroscopic properties. As shown in Ref. [41], this condition is satisfied in the grown crystals, so that the Lu^{3+} doping level is about x = 0.05–0.1, i.e., the compositions $Ca(Gd_{0.9-0.95}Lu_{0.1-0.05})AlO_4$ can be taken as the lower limit of the solid-solution definition.

It is not clear yet what is the upper limit (x) for the existence of such a solid solution. The single crystal growth of $CaLuAlO_4$ has never been

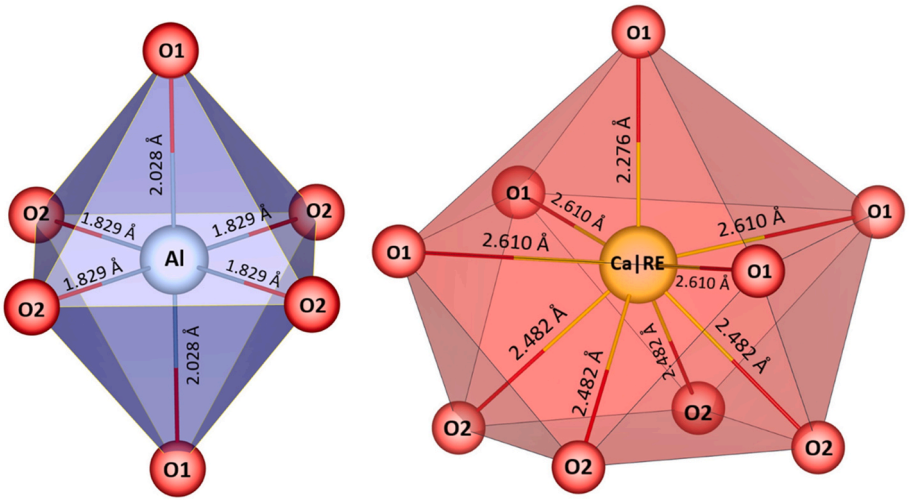

Fig. 6. Schematic of the [AlO_6] (left) and [Ca|REO_9] (right) polyhedra in the structure of Tm,Ho:CALGLO (batch #1).

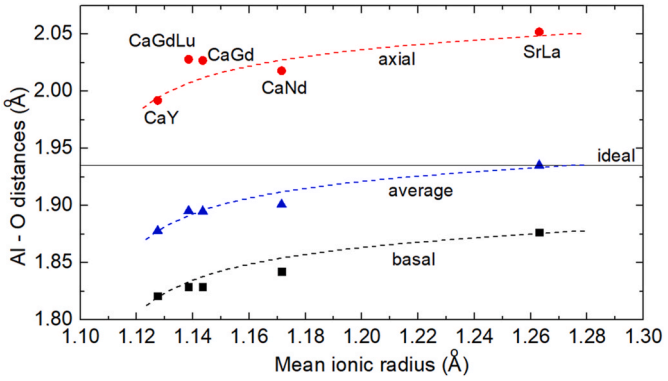

Fig. 7. Al – O interatomic distances in [AlO_6] octahedra for MM'AlO_4 crystals with K_2NiF_4-type structure versus the mean ionic radius of M^{2+} and M'^{3+} cations (the data from the present work and Ref. [4]). Horizontal line – ideal Al – O distance calculated from the ionic radii of VI-fold coordinated Al^{3+} and O^{2-}.

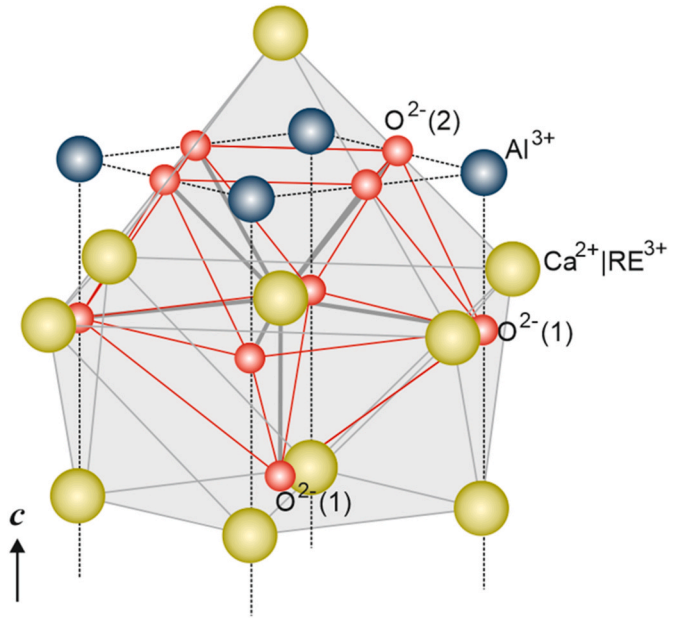

Fig. 8. Second coordination sphere of Tm^{3+}|Ho^{3+} ions by Ca^{2+}|RE^{3+} cations in Tm,Ho:CALGLO.

reported in the literature. In Ref. [26], the author attempted to grow $CaLuAlO_4$ using the standard procedure for $CaGdAlO_4$ resulting in polycrystalline, fine-grained, needle-like body of orange-red color with only the cubic Lu_2O_3 structure reliably identified. He concluded that $CaLuAlO_4$, if it exists at all, melts incongruently and the phase relationships in the CaO-Lu_2O_3–Al_2O_3 system differ greatly from those for the CaO-Gd_2O_3–Al_2O_3 one.

The stability of $ABCO_4$ crystals can be assessed from the following considerations. The ionic radii of the A^{2+} and B^{3+} cations provide the information about the deviation from the ideal perovskite lattice (for the P "phase"). Such a deviation will cause deformations in and between the P and S "phase" layers. For BCO_3 crystals with a perovskite structure, the so-called Goldschmidt's tolerance factor t is given by Ref. [42]:

$$t = \frac{R(B^{3+}) + R(O^{2-})}{\sqrt{2}(R(C^{3+}) + R(O^{2-}))}. \quad (1)$$

It is used to assess the geometric stability and distortion of BCO_3 crystal structures in terms of the constituent ionic packing. An ideal perovskite compounds adopts a cubic close packed structure with $t = 1$. When the ratio of the ionic radii deviates from the ideal value (so that $t \neq 1$, representing a loosely packed or tightly packed structure in the case of $t < 1$ and $t > 1$, respectively), a geometric strain and crystal distortions arise. With higher deviation from the t = 1 value, the crystal adopts structures of lower symmetries. Thus, t can be used to estimate the compatibility of different ions within a crystalline structure and to evaluate its geometric strain and stability [43]. Taking into account the statistical distribution of A^{2+} and C^{3+} cations in the tetragonal $ABCO_4$ crystals, we should replace $R(B^{3+})$ by $(R(A^{2+}) + R(B^{3+}))/2$ [26].

Liebald analyzed the stability of various compounds of the $ABCO_4$ family possessing the K_2NiF_4 type structure [26]. Due to the presence of P layers in the structure, the range of tolerance factors $t > 0.9$ similar to free perovskite was assumed. As $CaLaAlO_4$ ($t = 0.9494$) is unstable [44], all the t values above 0.95 are considered to correspond to unstable structures. The lower limit for t is placed by $CaNdGdO_4$ ($t = 0.9002$) which is orthorhombic; a certain margin ($t < 0.92$) is assumed. Thus, the compounds with $0.92 < t < 0.95$ are concluded to be most stable. For $CaGdAlO_4$ and $CaYAlO_4$, $t = 0.9295$ and 0.9236, respectively, i.e., well satisfying this condition, while for hypothetically existing $CaLuAlO_4$, $t = 0.9157$. Lower t values mean a strong distortion in the P-positions parallel to the ***a*** - ***b*** plane of the crystal structure. Since compounds with an ilmenite ($FeTiO_3$) type structure are formed for very small t values, the formation of a different crystal structure for $ABCO_4$ compounds with decreasing t probably represents a reaction of the K_2NiF_4 structure to the

distortion of the P layers.

From Eq. (1), modified for the case of $ABCO_4$ crystals and the above-mentioned range for tolerance factors, we estimate the maximum content of Lu^{3+} in the $CaGd_{1-x}Lu_xAlO_4$ solid solution as $x = 0.7$. While this is a rough estimation, we expect that stable solid-solutions with Lu^{3+} content up to few tens of at.% may exist.

4.3. Raman spectroscopy

The factor group analysis [45] for the primitive cell of the D^{17}_{4h} symmetry predicts the following set of irreducible representations at the center of the Brillouin zone ($\boldsymbol{k} = 0$): $\Gamma = 2A_{1g} + 2E_g + 4A_{2u} + 5E_u + B_{2u}$ [46]. Four Raman active modes are all even species involving vibrations of mainly one type of atoms: $A_{1g} + E_g$ modes of Ca|RE and $A_g + E_g$ modes of O; 11 IR-active modes are $3A_{2u} + 4E_u$; two modes ($A_{2u} + E_u$) are acoustic and one (B_{2u}) is silent [46,47].

The polarized Raman spectra of the Tm,Ho:CALGLO crystal (batch #1) are shown in Fig. 9. They were measured using both ***a***-cut and ***c***-cut samples. In Fig. 9, we use Porto's notations [48]: $m(nk)\bar{l}$, where m and l are the directions of propagation of the incident and scattered light, respectively (in our case for the confocal geometry, $m \equiv l$), and n and k are the polarization states of the incident and scattered light, respectively. Thus, five spectra were measured, $a(nk)\bar{a}$, where $n, k = \pi$ or σ and $c(\sigma\sigma)\bar{c}$. The Raman spectra are strongly polarized.

In the spectra taken for ***a***-cut crystals, all the Raman-active modes should appear: the $a(\pi\pi)\bar{a}$ geometry selects the A_{1g} phonons, and in the $a(\pi\sigma)\bar{a}$ geometry, the E_g modes appear. For the E_g geometry, as expected, only two intense modes at ~154 and 313 cm^{-1} appear [46]. The low-frequency mode is assigned to Ca|RE vibrations in the ***a-b*** plane and the high-frequency one – to the similar O vibrations. For the $a(\sigma\sigma)\bar{a}$ A_{1g} geometry, another band at even higher frequencies with two maxima, at 514 and 542 cm^{-1}, appears and it is assigned to O vibrations. For the $a(\pi\pi)\bar{a}$ A_{1g} geometry, the spectrum presents the most intense band at 311 cm^{-1} and a weaker band at ~542 cm^{-1}. The band at ~311 cm^{-1} is thus assigned to A_{1g} symmetry (Ca|RE vibrations along the ***c***-axis) and the band with a complex structure (clearly revealed for the $a(\sigma\sigma)\bar{a}$ geometry) with two maxima at ~514 and 542 cm^{-1} – to O vibrations. Note that the energy of the most intense mode is very different from the case of the isostructural $SrLaAlO_4$ crystal for which the two A_{1g} modes are at 222 (very intense) and 512 cm^{-1} (weak). Thus, we identify all 4 Raman-active modes. The bands at ~615 and 650 cm^{-1} are probably due to defect-induced modes [46].

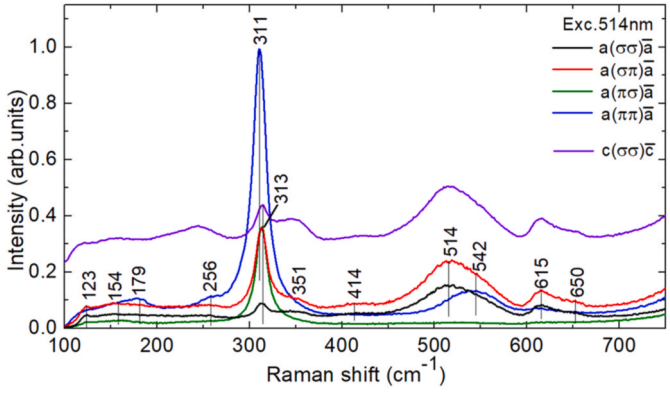

Fig. 9. Polarized Raman spectra of ***a***-cut and ***c***-cut Tm,Ho:CALGLO crystals (batch #1) (Porto's notations), λ_{exc} = 514 nm, *numbers* – Raman frequencies in cm^{-1}.

5. Optical absorption

5.1. Absorption spectra

The absorption spectra of the Tm,Ho:CALGLO crystal (batch #1) measured for π and σ light polarizations are shown in Fig. 10. The spectra contain bands assigned to Tm^{3+} dopant ions (the transitions from the $^3H_6$ ground-state to the excited-states from $^3F_4$ to $^1D_2$), as well as Ho^{3+} ones (the transitions from the $^5I_8$ ground-state to the excited-states from $^5I_7$ to $^3H_6$). In Fig. 10, the assignment of the Ho^{3+} multiplets is after [49]. In the UV, the sharp lines at 302–314 nm are due to optical absorption of the host-forming cations (Gd^{3+}, the $^8S_{7/2} \rightarrow {}^6P_{7/2}$ transition). The Lu^{3+} ions are optically inactive. In the visible, there is a broad structureless absorption band spanning from ~300 to 550 nm underlying the absorption of rare-earth ions. It is related to residual absorption of color centers.

5.2. Transition intensities of Ho^{3+} ions

The transition intensities of the Tm^{3+} ion in CALGLO crystals have been already analyzed [28]. In the present work, we focus on the Ho^{3+} ion. For this, the known absorption due to Tm^{3+} was subtracted from the spectra shown in Fig. 10. The Judd-Ofelt (J-O) formalism was applied to electric-dipole (ED) contributions to transition intensities. The contribution of magnetic-dipole (MD) transitions (for $\Delta J = J - J' = 0, \pm 1$, except for $J = J' = 0$) was calculated separately within the Russell–Saunders approximation on wave functions of Ho^{3+} under an assumption of a free-ion. The set of reduced squared matrix elements $U^{(k)}$ was taken from Ref. [50]. The dispersion curves of $CaGdAlO_4$ reported in Ref. [8] were used. All the values were considered as polarization-averaged, $<..> = (2\sigma + \pi)/3$.

The absorption oscillator strengths were determined from the measured absorption spectra using:

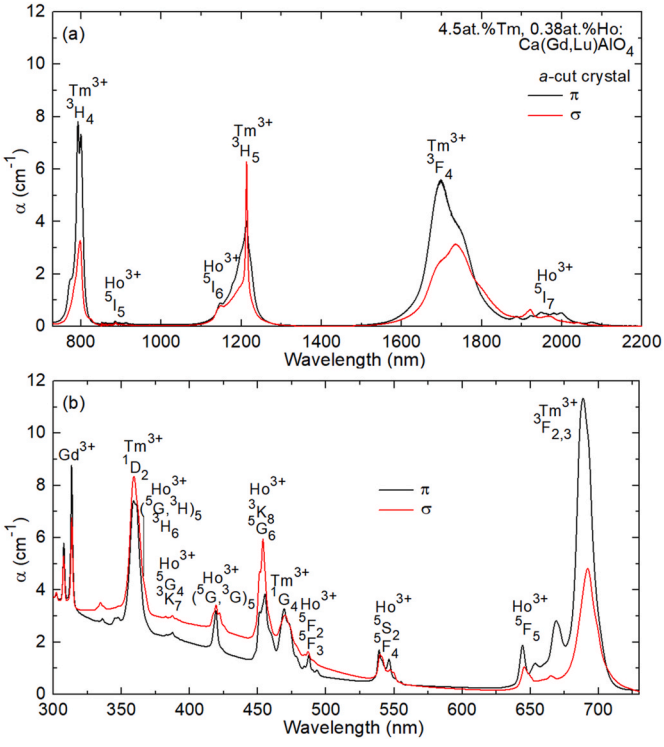

Fig. 10. Polarized absorption spectra of a Tm,Ho:CALGLO crystal (batch #1) for π and σ light polarizations: (a) near-IR, (b) visible and UV.

$$<f_{\exp}(JJ')> = \frac{m_e c^2}{\pi e^2 N_{\mathrm{Ho}} \langle\lambda\rangle^2} < \Gamma(JJ') >, \quad (2)$$

where m_e and e are the electron mass and charge, respectively, c is the speed of light, $<\Gamma(JJ')>$ is the integrated absorption coefficient within the absorption band and $\langle\lambda\rangle$ is the "center of gravity" of the absorption band. The results are shown in Table 5.

In the standard J-O theory, the ED line strengths of the J → J′ transitions $S^{ED}(JJ')$ are given by Refs. [51,52]:

$$S^{ED}_{calc}(JJ') = \sum_{k=2,4,6} U^{(k)} \Omega_k, \quad (3a)$$

$$U^{(k)} = \langle (4f^n) SLJ || U^k || (4f^n) S'L'J' \rangle^2. \quad (3b)$$

Here, $U^{(k)}$ are the reduced squared matrix elements and Ω_k are the intensity (J–O) parameters ($k = 2, 4, 6$).

Let us take into account the possible configuration interaction. If only the lower-energy excited configuration of the opposite parity ($4f^{n-1}5\,d^1 = 4f^9 5\,d^1$ for Ho^{3+}) contributes to the configuration interaction, the ED line strengths are [53]:

$$S^{ED}_{calc}(JJ') = \sum_{k=2,4,6} U^{(k)} \widetilde{\Omega}_k, \quad (4a)$$

$$\widetilde{\Omega}_k = \Omega_k [1 + 2\alpha(E_J + E_{J'} - 2E_f^0)]. \quad (4b)$$

Here, the intensity parameters $\widetilde{\Omega}_k$ are the linear functions of energies (E_J and $E_{J'}$) of the two multiplets involved in the transition J → J′, E_f^0 is the mean energy of the $4f^n$ configuration and $\alpha \approx 1/(2\Delta)$, where Δ has the meaning of the average energy difference between the $4f^n$ and $4f^{n-1}5\,d^1$ configurations. This approximation is typically referred to as the modified Judd-Ofelt (mJ-O) theory [53,54]. The $\widetilde{\Omega}_k$ parameters for the mJ-O theory are transformed into Ω_k ones for the standard theory assuming a high-lying $4f^{n-1}5\,d^1$ excited electronic configuration (i.e., the energy difference Δ → ∞ or, equivalently, $\alpha \to 0$).

The absorption oscillator strengths are related to the line strengths:

$$f^{\Sigma}_{calc}(JJ') = \frac{8}{3h(2J+1)\langle\lambda\rangle} \frac{(n^2+2)^2}{9n} S^{ED}_{calc}(JJ') + f^{MD}_{calc}(JJ'), \quad (5)$$

where h is the Planck constant, n is the refractive index of the crystal at $\langle\lambda\rangle$ and the superscript "Σ" stands for the total (ED + MD) value. In the standard J-O theory, there are three free parameters, (Ω_2, Ω_4, Ω_6), and in the mJ-O theory, there are four free parameters, (Ω_2, Ω_4, Ω_6 and α).

Let us discuss in detail the meaning of the intensity parameters. The electronic states have wavefunctions described by spherical harmonics, thus having the parity of the angular quantum number. Regardless the number of electrons (n), all states in the $4f^n$ shell always have a definite parity. For a free ion, this means that the electric dipole f – f transitions are parity forbidden. The prohibition by parity on forced ED transitions is removed in the presence of a noncentrosymmetric perturbing field, e.g., a crystal field, due to an admixture of states of excited configurations of opposite parity (e.g., $4f^{n-1}5\,d^1$) to those of the ground configuration $4f^n$ owing to the odd terms of the crystal field.

The matrix elements of the electric dipole operator are calculated by considering the crystal field as a first-order perturbation. This calculation is simplified under the following assumptions: (i) the states of the ground $4f^n$ configuration are taken as linear combinations of Russell-Saunders coupled states (the intermediate coupling scheme); (ii) the ground $4f^n$ and the excited $4f^{n-1}5\,d^1$ configurations are completely degenerated and the excited configuration is located much higher than the ground one, so that its effect on all the multiplets of the ground configuration is identical, (iii) all the Stark sub-levels of the ground manifold are equally populated and (iv) the local field approximation applies. In this case, the line strengths of electric dipole f – f transitions are described by Eq. (3) and the set of intensity parameters (Ω_k) is identical for all the transitions. Such an assumption describes weak configuration interaction (WCI) or standard J-O theory.

The intensity parameters (Ω_k) contain the odd-order parameters of the crystal-field, radial integrals of wavefunctions of the ground $4f^n$ and perturbing configurations, *etc*. In principle, it is possible to calculate the (Ω_k) parameters *ab initio*, however, they are usually considered as a set of phenomenological parameters fitting the experimental absorption data [55].

The mJ-O theory is accounting for the fact that different multiplets of the ground configuration have different energies and, consequently, different energy gaps with respect to the excited configuration of opposite parity $4f^{n-1}5\,d^1$ (which is considered to be completely degenerated). In this case, the intensity parameters should depend on the energy of the two multiplets involved in the transition, as well as the average energy gap between the $4f^n$ and $4f^{n-1}5\,d^1$ configurations, as represented by Eq. (4b).

Note that one of the main assumptions of the standard Judd-Ofelt theory (the energy gap between the ground configuration $4f^n$ and any excited configuration is much higher than the energies of the multiplets involved in the considered transition) is violated for almost all the trivalent rare-earth ions except of Yb^{3+} and Ce^{3+}. It is especially clear for higher lying $4f^n$ multiplets. Thus, strictly speaking, the configuration interaction should be considered for all these ions (including Ho^{3+} ones studied in the present work). Note that the effect of excited configurations is especially evident for Pr^{3+} ions for which the standard J-O theory fails to explain the experimental transition intensities. The explanation of the particular case of Pr^{3+} can be found elsewhere [56].

For the analysis, a total of 8 Ho^{3+} transitions in the CALGLO crystal were considered. The calculated absorption oscillator strengths are listed in Table 5. Both the J-O and the mJ-O theories provide close root-mean-square (r.m.s.) deviations between $<f_{exp}>$ and f^{Σ}_{calc}, namely 2.949 and 3.025, respectively. However, the mJ-O theory better describes the transition to the metastable Ho^{3+} excited-state ($^5I_7$), compare $<f_{exp}> = 2.808 \times 10^{-6}$ with $f^{\Sigma}_{calc} = 5.027 \times 10^{-6}$ (J-O) and 4.265×10^{-6} (mJ-O). Thus, it was selected for further analysis.

The obtained intensity parameters are listed in Table 6. For the mJ-O

Table 5
Experimental and calculated absorption oscillator strengths[a] for Ho^{3+} ions in Tm,Ho:CALGLO crystals.

$^5I_8 \to {}^{2S+1}L_J$	$<\lambda>$, nm	$<\Gamma>$, $cm^{-1}nm$	$<f_{exp}>$, 10^{-6}	f^{Σ}_{calc}, 10^{-6} J–O	mJ-O
$^5I_7$	1935	37.27	2.808	$4.459^{ED} + 0.568^{MD}$	$3.697^{ED} + 0.568^{MD}$
$^5I_6$	1162	30.34	5.156	3.049^{ED}	2.829^{ED}
$^5I_5$	898	2.03	0.610	0.585^{ED}	0.568^{ED}
$^5F_5$	772	30.75	16.835	12.391^{ED}	11.367^{ED}
$^5S_2 + {}^5F_4$	656	13.81	11.327	13.430^{ED}	14.187^{ED}
$^5F_3 + {}^5F_2 + {}^3K_8 + {}^5G_6$	544	56.36	62.272	$63.291^{ED} + 0.126^{MD}$	$62.984^{ED} + 0.126^{MD}$
$^5G1_5$	467	9.81	13.455	16.470^{ED}	16.015^{ED}
$^5G2_5 + {}^3H_6 + {}^3F_2$	422	13.20	24.592	19.528^{ED}	21.247^{ED}
r.m.s. dev.				*2.949*	*3.025*

[a] $<\lambda>$ – "center of gravity" of an absorption band, $<\Gamma>$ – integrated absorption coefficient, $<f_{exp}>$ and f^{Σ}_{calc} – experimental and calculated absorption oscillator strengths, respectively, ED and MD stand for the electric-dipole and magnetic-dipole contributions, respectively, <> stand for polarization-averaging, $(2\sigma + \pi)/3$.

Table 6
Intensity parameters of Ho^{3+} ions in CALGLO.

Parameter	J-O theory	mJ-O theory
$\Omega_2 \times 10^{20}$, cm^2	8.899	11.221
$\Omega_4 \times 10^{20}$, cm^2	11.194	13.586
$\Omega_6 \times 10^{20}$, cm^2	3.685	6.048
$\alpha \times 10^4$, cm	–	0.070

theory, they are $\Omega_2 = 11.221$, $\Omega_4 = 13.586$ and $\Omega_6 = 6.048$ [10^{-20} cm^2] and $\alpha = 0.070$ [10^{-4} cm], and the phenomenological parameter $\Delta = 1/(2\alpha) = 14.3 \times 10^4$ cm^{-1} (high-lying excited configuration).

The probabilities of radiative spontaneous transitions for emission channels J → J′ are then determined from the corresponding line strengths in emission:

$$A^{\Sigma}_{calc}(JJ') = \frac{64\pi^4 e^2}{3h(2J+1)\langle\lambda\rangle^3} n\left(\frac{n^2+2}{3}\right)^2 S^{ED}_{calc}(JJ') + A^{MD}_{calc}(JJ'). \quad (6)$$

Using the A_{calc} values, we have further determined the total probabilities of spontaneous radiative transitions from the excited states A_{tot}, the corresponding radiative lifetimes τ_{rad} and the luminescence branching ratios for the particular emission channels $B(JJ')$:

$$\tau_{rad} = \frac{1}{A_{tot}}, \text{ Where } A_{tot} = \sum_{J'} A^{\Sigma}_{calc}(JJ'); \quad (7a)$$

$$B(JJ') = \frac{A^{\Sigma}_{calc}(JJ')}{A_{tot}}, \quad (7b)$$

The results are shown in Table 7. They are obtained using the mJ-O theory. For the $^5I_7$ Ho^{3+} multiplet, τ_{rad} is 3.32 ms. Considering the residual difference between the $\langle f_{exp}\rangle$ and f^{Σ}_{calc} values for the $^5I_8 \rightarrow {}^5I_7$ transition in absorption, the upper limit for the estimated radiative lifetime of the $^5I_7$ state is 5.04 ms.

Previously, for the Ho:$CaGdAlO_4$ crystal, the following J-O parameters were reported: $\Omega_2 = 3.65$, $\Omega_4 = 3.79$ and $\Omega_6 = 4.17$ [10^{-20} cm^2] [18] leading to the radiative lifetime of the $^5I_7$ state of 3.84 ms which reasonably agrees with our data.

In the present work, the transition intensities for Ho^{3+} ions were calculated based on the analysis of directly measured absorption spectra (a classical approach). For non-transparent materials for which the absorption data can be unavailable, other approaches are used based on the analysis of either (i) excitation or diffuse-reflection spectra [57,58], (ii) luminescence spectra for certain RE^{3+} ions with purely MD transitions [59,60] or even (iii) luminescence decay curves [61].

5.3. IR transmission spectrum

The IR transmission spectrum of a ***c***-cut Tm,Ho:CALGLO crystal (batch #2) is shown in Fig. 11. The crystal exhibits a relatively broad transparency range (for oxide crystals), the IR absorption edge is found at 6.7 μm.

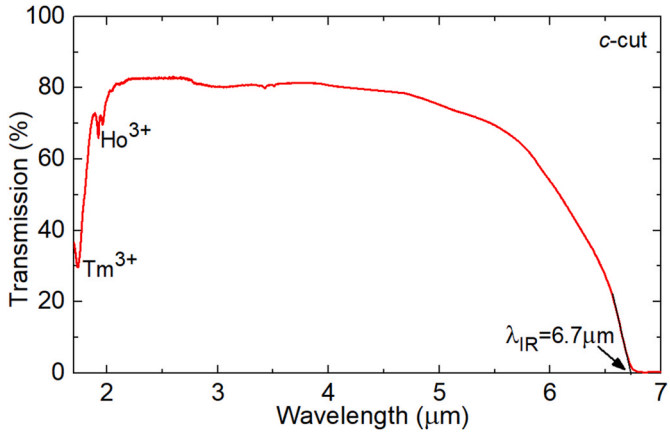

Fig. 11. IR transmission spectrum of a ***c***-cut Tm,Ho:CALGLO crystal (batch #2).

The broad transparency range of Tm,Ho:CALGLO crystals extending far in the IR, as well as their low-phonon-energy behavior leading to weak non-radiative path for the dopant rare-earth ions make them interesting for applications in lasers emitting above 2 μm (in the mid-IR spectral range). Note that originally, these crystals were grown for exploiting the $^3F_4 \rightarrow {}^3H_6$ Tm^{3+} and $^5I_7 \rightarrow {}^5I_8$ Ho^{3+} laser transitions around 2 μm. Other promising transitions of these ions are $^3H_4 \rightarrow {}^3H_5$ (Tm^{3+}, at ~2.3 μm) and $^5I_6 \rightarrow {}^5I_7$ (Ho^{3+}, at ~3 μm).

6. Conclusions

To conclude, we explored the formation of substitutional solid-solutions in the system $CaGd_{1-x}Lu_xAlO_4$ as laser host materials for doping with laser-active Tm^{3+} and Ho^{3+} ions. The crystals of Tm,Ho:CALGLO with Lu^{3+} content up to 10.8 at.% (which is almost twice higher than in the previous studies for other laser-active rare-earth dopants) are grown by the Cz method using [001]-oriented seeds from $CaGdAlO_4$. The segregation coefficients for rare-earth ions (Lu^{3+}, Tm^{3+} and Ho^{3+}) are determined and correlated with their ionic radii

Table 7
Calculated probabilities of spontaneous radiative transitions[a] of Ho^{3+} ions in CALGLO (the mJ-O theory).

Emitting state	Terminal state	$\langle\lambda\rangle$, nm	$A^{\Sigma}_{calc}(JJ')$, s^{-1}	$B(JJ')$	A_{tot}, s^{-1}	τ_{rad}, ms
$^5I_7$	$^5I_8$	1935	$273.0^{ED}+42.0^{MD}$	1	301.5	3.32
$^5I_6$	$^5I_7$	2909	$76.9^{ED}+20.4^{MD}$	0.137	763.6	1.31
	$^5I_8$	1162	654.6^{ED}	0.863		
$^5I_5$	$^5I_6$	3964	$33.9^{ED}+9.5^{MD}$	0.063	584.1	1.46
	$^5I_7$	1678	364.8^{ED}	0.554		
	$^5I_8$	898	262.9^{ED}	0.383		
$^5I_4$	$^5I_5$	5507	$28.4^{ED}+4.2^{MD}$	0.073	452.2	2.21
	$^5I_6$	2305	177.2^{ED}	0.391		
	$^5I_7$	1286	198.1^{ED}	0.451		
	$^5I_8$	772	38.5^{ED}	0.085		
$^5F_5$	$^5I_4$	4354	$0.5^{ED}+0.03^{MD}$	<0.001	13235	0.076
	$^5I_5$	2431	$44.2^{ED}+0.8^{MD}$	0.002		
	$^5I_6$	1507	$553.7^{ED}+2.8^{MD}$	0.028		
	$^5I_7$	993	2682^{ED}	0.171		
	$^5I_8$	656	10230^{ED}	0.799		
$^5S_2+{}^5F_4$	$^5F_5$	3191	$57.7^{ED}+6.8^{MD}$	<0.001	36993	0.021
	$^5I_4$	1841	$394.9^{ED}+0.07^{MD}$	0.021		
	$^5I_5$	1380	$1125^{ED}+0.3^{MD}$	0.019		
	$^5I_6$	1023	3062^{ED}	0.078		
	$^5I_7$	757	7490^{ED}	0.380		
	$^5I_8$	544	24901^{ED}	0.502		

[a] $\langle\lambda\rangle$ – mean emission wavelength of the emission band, $A^{\Sigma}_{calc}(JJ')$ – probability of radiative spontaneous transition, $B(JJ')$ – luminescence branching ratio, A_{tot} and τ_{rad} – total probability of radiative spontaneous transitions and the radiative lifetime, respectively, ED and MD stand for the electric-dipole and magnetic-dipole contributions, respectively.

suggesting an empirical formula. The Tm,Ho:CALGLO crystals maintain the tetragonal (K_2NiF_4-type, sp. gr. *I4/mmm*) structure. The Rietveld refinement data include the fractional atomic coordinates and interatomic distances. The first (by oxygen) and second (by $Ca^{2+}|RE^{3+}$ cations) coordination spheres of rare-earth sites are described. The low-phonon-energy vibronic behavior of Tm,Ho:CALGLO crystals is revealed. The most intense Raman mode is found at 311 cm^{-1} (assigned to A_{1g} symmetry) and the maximum phonon frequency is ~650 cm^{-1}. The polarized absorption spectra of Tm,Ho:CALGLO crystals are systematically studied. The Ho^{3+} transition probabilities are described using the modified Judd-Ofelt (mJ-O) theory accounting for the configuration interaction.

Future work regarding the growth of rare-earth-doped CALGLO crystals should focus on exploiting the limit of stability of the $CaGd_{1-x}Lu_xAlO_4$ solution. In the present work, using the Goldschmidt's tolerance factor *t* modified for the $ABCO_4$ structure, we estimated the upper limit of stability to be x ~0.7. The introduction of even higher Lu^{3+} content may greatly promote the spectral broadening for dopant ions and facilitate their segregation factors (as the difference of ionic radii of $Yb^{3+}|Tm^{3+}|Ho^{3+}$ and Lu^{3+} is smaller as compared with Gd^{3+}). Indeed, in the present work, the introduction of 10.8 at.% Lu^{3+} resulted in increased Tm^{3+} segregation coefficient $K_{Tm} = 0.90$, compared with its value of ~0.6 for the parent compound, $CaGdAlO_4$.

Credit author statement

Zhongben Pan: Investigation, Pavel Loiko: Conceptualization, Writing – original draft, Investigation, Sami Slimi: Investigation, Writing – original draft, Hualei Yuan: Investigation, Yicheng Wang: Investigation, Yongguang Zhao: Investigation, Patrice Camy: Supervision, Elena Dunina: Investigation, Alexey Kornienko: Investigation, Liudmila Fomicheva: Investigation, Li Wang: Investigation, Weidong Chen: Writing – original draft, Uwe Grieber: Supervision, Valentin Petrov: Writing – review & editing, Rosa Maria Solé; : Data curation, Investigation, Magdalena Aguiló; : Funding acquisition, Supervision Francesc Díaz: Funding acquisition, Xavier Mateos: Conceptualization, Writing – review & editing, Investigation.

Declaration of competing interest

The authors declare that they have no known competing financial interests or personal relationships that could have appeared to influence the work reported in this paper.

Acknowledgments

This work was supported by the Spanish Government, Ministry of Science and Innovation (project No. PID2019-108543RB-I00) and by the Generalitat de Catalunya (project No. 2017SGR755). Y. Zhao acknowledges financial support from the Alexander von Humboldt Foundation through a Humboldt fellowship. National Natural Science Foundation of China (52072351). China Academy of Engineering Physics (CAEP) (YZJJLX2018005). Fund of Key Laboratory of Optoelectronic Materials Chemistry and Physics, Chinese Academy of Sciences (2008DP173016). Qilu Young Scholar Program of Shandong University. The Science Foundation of Fujian Province (2019J02015). Foundation of State Key Laboratory of Crystal Materials, Shandong University (KF2001).

References

[1] J. Petit, P. Goldner, B. Viana, Laser emission with low quantum defect in Yb: $CaGdAlO_4$, Opt. Lett. 30 (2005) 1345–1347.
[2] J.A. Hutchinson, H.R. Verdun, B.H. Chai, B. Zandi, L.D. Merkle, Spectroscopic evaluation of $CaYAlO_4$ doped with trivalent Er, Tm, Yb and Ho for eyesafe laser applications, Opt. Mater. 3 (1994) 287–306.
[3] R. Moncorgé, N. Garnier, P. Kerbrat, C. Wyon, C. Borel, Spectroscopic investigation and two-micron laser performance of Tm^{3+}:$CaYAlO_4$ single crystals, Opt Commun. 141 (1997) 29–34.
[4] R.D. Shannon, R.A. Oswald, J.B. Parise, B.H.T. Chai, P. Byszewski, A. Pajaczkowska, R. Sobolewski, Dielectric constants and crystal structures of $CaYAlO_4$, $CaNdAlO_4$, and $SrLaAlO_4$, and deviations from the oxide additivity rule, J. Solid State Chem. 98 (1992) 90–98.
[5] L. Vasylechko, N. Kodama, A. Matkovskii, Y. Zhydachevskii, Crystal structure and optical spectroscopy of $CaGdAlO_4$:Er single crystal, J. Alloys Compd. 300 (2000) 475–478.
[6] P.O. Petit, J. Petit, P. Goldner, B. Viana, Inhomogeneous broadening of optical transitions in Yb:$CaYAlO_4$, Opt. Mater. 30 (2008) 1093–1097.
[7] P. Loiko, F. Druon, P. Georges, B. Viana, K. Yumashev, Thermo-optic characterization of Yb:$CaGdAlO_4$ laser crystal, Opt. Mater. Express 4 (2014) 2241–2249.
[8] P. Loiko, P. Becker, L. Bohatý, C. Liebald, M. Peltz, S. Vernay, D. Rytz, J.M. Serres, X. Mateos, Y. Wang, X. Xu, J. Xu, A. Major, A. Baranov, U. Griebner, V. Petrov, Sellmeier equations, group velocity dispersion and thermo-optic dispersion formulas for $CaLnAlO_4$ (Ln =Y, Gd) laser host crystals, Opt. Lett. 42 (2017) 2275–2278.
[9] P. Loiko, J.M. Serres, X. Mateos, X. Xu, J. Xu, V. Jambunathan, P. Navratil, A. Lucianetti, T. Mocek, X. Zhang, U. Griebner, V. Petrov, M. Aguiló, F. Díaz, A. Major, Microchip Yb, $CaLnAlO_4$ lasers with up to 91% slope efficiency, Opt. Lett. 42 (2017) 2431–2434.
[10] D. Li, X. Xu, Y. Cheng, S. Cheng, D. Zhou, F. Wu, C. Xia, J. Xu, J. Zhang, Crystal growth and spectroscopic properties of Yb:$CaYAlO_4$ single crystal, J. Cryst. Growth 312 (2010) 2117–2121.
[11] Y. Zaouter, J. Didierjean, F. Balembois, G. Lucas Leclin, F. Druon, P. Georges, J. Petit, P. Goldner, B. Viana, 47-fs diode-pumped Yb^{3+}:$CaGdAlO_4$ laser, Opt. Lett. 31 (2006) 119–121.
[12] P. Sévillano, P. Georges, F. Druon, D. Descamps, E. Cormier, 32-fs Kerr-lens mode-locked Yb:$CaGdAlO_4$ oscillator optically pumped by a bright fiber laser, Opt. Lett. 39 (2014) 6001–6004.
[13] F. Druon, M. Olivier, A. Jaffrès, P. Loiseau, N. Aubry, J. DidierJean, F. Balembois, B. Viana, P. Georges, Magic mode switching in Yb:$CaGdAlO_4$ laser under high pump power, Opt. Lett. 38 (2013) 4138–4141.
[14] K. Beil, B. Deppe, C. Kränkel, Yb:$CaGdAlO_4$ thin-disk laser with 70% slope efficiency and 90 nm wavelength tuning range, Opt. Lett. 38 (2013) 1966–1968.
[15] A. Diebold, F. Emaury, C. Schriber, M. Golling, C.J. Saraceno, T. Südmeyer, U. Keller, SESAM mode-locked Yb:$CaGdAlO_4$ thin disk laser with 62 fs pulse generation, Opt. Lett. 38 (2013) 3842–3845.
[16] Y. Wang, G. Xie, X. Xu, J. Di, Z. Qin, S. Suomalainen, M. Guina, A. Härkönen, A. Agnesi, U. Griebner, X. Mateos, P. Loiko, V. Petrov, SESAM mode-locked Tm:CALGO laser at 2 μm, Opt. Mater. Express 6 (2016) 131–136.
[17] Y. Zhao, Y. Wang, X. Zhang, X. Mateos, Z. Pan, P. Loiko, W. Zhou, X. Xu, J. Xu, D. Shen, S. Suomalainen, A. Härkönen, M. Guina, U. Griebner, V. Petrov, 87 fs mode-locked Tm,Ho:$CaYAlO_4$ laser at ~2043 nm, Opt. Lett. 43 (2018) 915–918.
[18] J. Di, X. Xu, C. Xia, Q. Sai, D. Zhou, Z. Lv, J. Xu, Growth and spectra properties of Tm, Ho doped and Tm, Ho co-doped $CaGdAlO_4$ crystals, J. Lumin. 155 (2014) 101–107.
[19] A. Pajaczkowska, A. Gloubokov, Synthesis, growth and characterization of tetragonal $ABCO_4$ crystals, Prog. Cryst. Growth Char. Mater. 36 (1998) 123–162.
[20] Z. Pan, X. Dai, Y. Lei, H. Cai, J.M. Serres, M. Aguiló, F. Díaz, J. Ma, D. Tang, E. Vilejshikova, U. Griebner, V. Petrov, P. Loiko, X. Mateos, Crystal growth and properties of the disordered crystal Yb:$SrLaAlO_4$: a promising candidate for high-power ultrashort pulse lasers, CrystEngComm 20 (2018) 3388–3395.
[21] A. Dabkowski, H.A. Dabkowski, J.E. Greedan, $SrLaGaO_4$-Czochralski crystal growth and basic properties, J. Cryst. Growth 132 (1993) 205–208.
[22] A. Novoselov, G. Zimina, L. Komissarova, A. Pajaczkowska, Synthesis and characterization of solid solutions in $ABCO_4$ system, J. Cryst. Growth 287 (2006) 305–308.
[23] F. Guo, Q. Xie, L. Qiu, B. Zhao, X. Chen, J. Chen, Growth, magnetic and magneto-optical properties of $CaDyAlO_4$ crystals, Opt. Mater. 112 (2021) 110719.
[24] M. Mei, L.L. Cao, Y. He, R.R. Zhang, F.Y. Guo, N.F. Zhuang, J.Z. Chen, Growth and magneto-optical properties of $CaTbAlO_4$ crystal, Adv. Mater. Res. 306 (2011) 1722–1727.
[25] K. Beil, S.T. Fredrich-Thornton, F. Tellkamp, R. Peters, C. Kränkel, K. Petermann, G. Huber, Thermal and laser properties of Yb:LuAG for kW thin disk lasers, Opt Express 18 (2010) 20712–20722.
[26] C. Liebald, Yb-dotierte Ultrakurzpuls-Lasermaterialien mit K_2NiF_4-Struktur - Züchtung und Verbesserung der Kristallqualität, Doctoral dissertation, Johannes Gutenberg-Universität Mainz, 2017 [in German].
[27] Q. Hu, Z. Jia, A. Volpi, S. Veronesi, M. Tonelli, X. Tao, Crystal growth and spectral broadening of a promising Yb:$CaLu_xGd_{1-x}AlO_4$ disordered crystal for ultrafast laser application, CrystEngComm 19 (2017) 1643–1647.
[28] Z. Pan, P. Loiko, J.M. Serres, E. Kifle, H. Yuan, X. Dai, H. Cai, Y. Wang, Y. Zhao, M. Aguiló, F. Díaz, U. Griebner, V. Petrov, X. Mateos, Mixed" Tm:Ca(Gd,Lu)AlO_4 — a novel crystal for tunable and mode-locked 2 μm lasers, Opt Express 27 (2019) 9987–9995.
[29] H. Bernhardt, On the coloration behaviour of undoped $YAlO_3$ crystals, Phys. Status Solidi 21 (1974) 95–98.
[30] Q. Hu, Z. Jia, C. Tang, N. Lin, J. Zhang, N. Jia, S. Wang, X. Zhao, X. Tao, The origin of coloration of $CaGdAlO_4$ crystals and its effect on their physical properties, CrystEngComm 19 (2017) 537–545.

[31] A. Pajaczkowska, A. Gloubokov, A. Klos, C.F. Woensdregt, Czochralski growth of $SrLaAlO_4$ and $SrLaGaO_4$ single crystals and its implications for the crystal morphology, J. Cryst. Growth 171 (1997) 387–391.

[32] R.D. Shannon, Revised effective ionic radii and systematic studies of interatomic distances in halides and chalcogenides, Acta Crystallogr. A 32 (1976) 751–767.

[33] J. Di, X. Sun, X. Xu, C. Xia, Q. Sai, H. Yu, Y. Wang, L. Zhu, Y. Gao, X. Guo, Growth and spectral characters of Nd:$CaGdAlO_4$ crystal, Eur. Phys. J. Appl. Phys. 74 (2016) 10501.

[34] Q. Hu, Z. Jia, S. Veronesi, J. Zhang, A. Sottile, M. Tonelli, E. Cavalli, X. Tao, Crystal growth and optimization of Pr:$CaGdAlO_4$ by the flux-Czochralski method, CrystEngComm 20 (2018) 590–596.

[35] R. Li, X. Xu, L. Su, Q. Sai, C. Xia, Q. Yang, J. Xu, A. Strzęp, A. Półkoszek, Crystal characterization and optical spectroscopy of Eu^{3+}-doped $CaGdAlO_4$ single crystal fabricated by the floating zone method, Chin. Opt Lett. 14 (2016), 021602.

[36] S. Li, Y. Yang, S. Zhang, T. Yan, N. Ye, Y. Hang, Enhanced 2.86 μm emission from a Ho, Pr:$CaGdAlO_4$ crystal, J. Lumin. 228 (2020) 117620.

[37] N. Zhang, H. Wang, Y. Yin, T. Wang, Z. Jia, J. Zhang, Q. Hu, N. Lin, X. Fu, X. Tao, Cracking mechanism and spectral properties of Er, Yb:$CaGdAlO_4$ crystals grown by the LHPG method, CrystEngComm 22 (2020) 955–960.

[38] K. Hasse, T. Calmano, B. Deppe, C. Liebald, C. Kränkel, Efficient Yb^{3+}:$CaGdAlO_4$ bulk and femtosecond-laser-written waveguide lasers, Opt. Lett. 40 (2015) 3552–3555.

[39] K. Subbotin, P. Loiko, S. Slimi, A. Volokitina, A. Titov, D. Lis, E. Chernova, S. Kuznetsov, R.M. Solé, U. Griebner, V. Petrov, M. Aguiló, F. Díaz, P. Camy, E. Zharikov, X. Mateos, Monoclinic zinc monotungstate Yb^{3+},Li^{+}:$ZnWO_4$: Part I. Czochralski growth, structure refinement and Raman spectra, J. Lumin. 228 (2020) 117601.

[40] I. Zvereva, Y. Smirnov, J. Choisnet, Demixion of the K_2NiF_4 type aluminate $LaCaAlO_4$: precursor role of the local ordering of lanthanum and calcium, Mater. Chem. Phys. 60 (1999) 63–69.

[41] Z. Pan, P. Loiko, J.M. Serres, H. Yuan, X. Dai, H. Cai, Y. Wang, Li Wang, Y. Zhao, R. M. Solé, M. Aguiló, F. Díaz, P. Camy, W. Chen, U. Griebner, V. Petrov, X. Mateos, Tm,Ho:Ca(Gd,Lu)AlO_4 crystals: optical spectroscopy and laser operation, J. Lumin. (2021), 118828. In press.

[42] V.M. Goldschmidt, Die Gesetze der Krystallochemie, Naturwissenschaften 21 (1926) 477–485.

[43] T. Sato, S. Takagi, S. Deledda, B.C. Hauback, S.I. Orimo, Extending the applicability of the Goldschmidt tolerance factor to arbitrary ionic compounds, Sci. Rep. 6 (2016), 23592-1-10.

[44] I. Zvereva, Y. Smirnov, J. Choisnet, Demixion of the K_2NiF_4 type aluminate $LaCaAlO_4$: precursor role of the local ordering of lanthanum and calcium, Mater. Chem. Phys. 60 (1999) 63–69.

[45] D.L. Rousseau, R.P. Bauman, S.P.S. Porto, Normal mode determination in crystals, J. Raman Spectrosc. 10 (1981) 253–290.

[46] V.G. Hadjiev, M. Cardona, I. Ivanov, V. Popov, M. Gyulmezov, M.N. Iliev, M. Berkowski, Optical phonons probe of the $SrLaAlO_4$ crystal structure, J. Alloys Compd. 251 (1997) 7–10.

[47] A.A. Kaminskii, X. Xu, O. Lux, H. Rhee, H.J. Eichler, J. Zhang, D. Zhou, A. Shirakawa, K. Ueda, J. Xu, High-order stimulated Raman scattering in tetragonal $CaYAlO_4$ crystal-host for Ln^{3+}-lasant ions, Laser Phys. Lett. 9 (2012) 306–311.

[48] T.C. Damen, S.P.S. Porto, B. Tell, Raman effect in zinc oxide, Phys. Rev. 142 (1966) 570–574.

[49] W.T. Carnall, P.R. Fields, K. Rajnak, Electronic energy levels in the trivalent lanthanide aquo ions. I. Pr^{3+}, Nd^{3+}, Pm^{3+}, Sm^{3+}, Dy^{3+}, Ho^{3+}, Er^{3+}, and Tm^{3+}, J. Chem. Phys. 49 (1968) 4424–4442.

[50] M.C. Pujol, C. Cascales, M. Rico, J. Massons, F. Dıaz, P. Porcher, C. Zaldo, Measurement and crystal field analysis of energy levels of Ho^{3+} and Er^{3+} in KGd$(WO_4)_2$ single crystal, J. Alloys Compd. 323 (2001) 321–325.

[51] B.R. Judd, Optical absorption intensities of rare-earth ions, Phys. Rev. 127 (1962) 750–761.

[52] G.S. Ofelt, Intensities of crystal spectra of rare-earth ions, J. Chem. Phys. 37 (1962) 511–520.

[53] A.A. Kornienko, A.A. Kaminskii, E.B. Dunina, Dependence of the line strength of f–f transitions on the manifold energy. II. Analysis of Pr^{3+} in $KPrP_4O_{12}$, Phys. Status Solidi B 157 (1990) 267–273.

[54] P. Loiko, A. Volokitina, X. Mateos, E. Dunina, A. Kornienko, E. Vilejshikova, M. Aguilo, F. Diaz, Spectroscopy of Tb^{3+} ions in monoclinic $KLu(WO_4)_2$ crystal: application of an intermediate configuration interaction theory, Opt. Mater. 78 (2018) 495–501.

[55] B.M. Walsh, Judd-Ofelt theory: principles and practices, in: Advances in Spectroscopy for Lasers and Sensing, Springer, Dordrecht, 2006, pp. 403–433.

[56] E.B. Dunina, L.A. Fomicheva, A.A. Kornienko, M.V. Grigoreva, Effect of configuration interaction of rare-earth ion states on the intensity of intermultiplet transitions, J. Appl. Spectrosc. 85 (2018) 407–415.

[57] W. Luo, J. Liao, R. Li, X. Chen, Determination of Judd–Ofelt intensity parameters from the excitation spectra for rare-earth doped luminescent materials, Phys. Chem. Chem. Phys. 12 (2010) 3276–3282.

[58] Y. Zhang, B. Chen, S. Xu, X. Li, J. Zhang, J. Sun, X. Zhang, H. Xia, R. Hua, A universal approach for calculating the Judd–Ofelt parameters of RE^{3+} in powdered phosphors and its application for the β-$NaYF_4$:Er^{3+}/Yb^{3+} phosphor derived from auto-combustion-assisted fluoridation, Phys. Chem. Chem. Phys. 20 (2018) 15876–15883.

[59] Y. Tian, B. Chen, R. Hua, J. Sun, L. Cheng, H. Zhong, X. Li, J. Zhang, Y. Zheng, T. Yu, L. Huang, H. Yu, Optical transition, electron-phonon coupling and fluorescent quenching of $La_2(MoO_4)_3$:Eu^{3+} phosphor, J. Appl. Phys. 109 (2011), 053511-1-6.

[60] A. Volokitina, P. Loiko, E. Vilejshikova, X. Mateos, E. Dunina, A. Kornienko, N. Kuleshov, A. Pavlyuk, Eu^{3+}:$KY(MoO_4)_2$: a novel anisotropic red-emitting material with a layered structure, J. Alloys Compd. 762 (2018) 786–796.

[61] M. Luo, B. Chen, X. Li, J. Zhang, S. Xu, X. Zhang, Y. Cao, J. Sun, Y. Zhang, X. Wang, Y. Zhang, D. Gao, L. Wang, Fluorescence decay route of optical transition calculation for trivalent rare earth ions and its application for Er^{3+}-doped $NaYF_4$ phosphor, Phys. Chem. Chem. Phys. 22 (2020) 25177–25183.